Pergamon

Int. J. Heat Mass Transfer. Vol. 38, No. 9, pp. 1683–1691, 1995

0017-9310/95 $9.50+0.00

0017-9310(94)00288-6

Linear stability of a double diffusive layer with variable fluid properties

JOSEF TANNY and VICTOR A. GOTLIB

Center for Technological Education Holon, P.O.B. 305, Holon 58102, Israel

(*Received* 10 *January* 1994 *and in final form* 10 *August* 1994)

Abstract—The linear stability of an infinite horizontal double diffusive layer stratified vertically by temperature and solute concentration is analyzed numerically for the case of temperature-dependent viscosity and salt diffusivity. The one-dimensional steady basic state associated with the variable properties is characterized by zero fluid velocity, a linear temperature profile and a non-linear salinity distribution. The horizontal boundaries are shear-free and perfectly conducting. The eigenvalue problem for the linearized perturbation equations is resolved numerically by the Galerkin method. The results for the direct mode ('finger regime') show that, in contrast to the constant properties case, the critical wavenumber increases with the solute Rayleigh number (Ra_S) and the critical thermal Rayleigh number is reduced from its corresponding constant properties value. The behavior of the oscillatory mode ('diffusive regime') is more complex, and two different branches exist for Ra_S larger than some fixed value. The least stable branch is characterized by a high wavenumber while the second branch by a small wavenumber.

1. INTRODUCTION

One of the fundamental problems of double diffusive convection is the stability of a statically stable horizontal fluid layer, stratified by two buoyancy components with different molecular diffusivities (e.g. heat and salt), which make opposite contributions to the overall vertical density distribution. In such systems, motion can arise even when the basic state density distribution is gravitationally stable [1]. The early theories pertinent to this problem (e.g. ref. [2]) analyzed the linear stability of a two-dimensional, infinite horizontal fluid layer with two constant vertical gradients of the buoyancy components, shear-free and perfectly conducting boundaries, and constant fluid properties. These theories have identified two distinct 'double diffusive instability' modes, depending on the relative distribution of the two buoyancy components.

When the faster diffusing component is stably distributed, instability emerges as direct steady convection in the form of long narrow salt fingers. The solution of the small perturbation equations yields an expression for Ra_T^0, the critical thermal Rayleigh number, as a function of Ra_S, the solute Rayleigh number:

$$Ra_T^0 = \frac{Ra_S}{\tau} + \frac{27\pi^4}{4}. \quad (1)$$

Here the zero superscript indicates the case of constant fluid properties and linear basic state profiles, $Ra_T = g\alpha\Delta Th^3/\nu k_T$, $Ra_S = g\beta\Delta Sh^3/\nu k_T$, g is the acceleration due to gravity, α and β are the positive coefficients of heat and solute expansion, respectively, ΔT and ΔS are the temperature and concentration differences across the layer of depth h, ν is the kinematic viscosity, k_T and k_S are the coefficients of molecular diffusivity of heat and salt, respectively, and $\tau = k_S/k_T$ is the diffusivity ratio. Another instability mode dominates when the faster diffusing buoyancy component is unstably distributed. In this case, the motion at the onset of instability is oscillatory and the minimum Ra_T^0 is

$$Ra_T^0 = \frac{Pr+\tau}{Pr+1} Ra_S + (1+\tau)\left(1+\frac{\tau}{Pr}\right)\frac{27\pi^4}{4} \quad (2)$$

where $Pr = \nu/k_T$ is the Prandtl number. The corresponding frequency of unstable oscillations is given by

$$p_i^2 = \tfrac{9}{4} Pr\left(\frac{\tau}{Pr}+\tau+1\right)\pi^4 - \frac{Pr}{3}(Ra_T^0 - Ra_S). \quad (3)$$

In both instability modes, Ra_T has a minimum critical value when the vertical wavenumber $n = 1$ and its corresponding horizontal wavenumber $a = \sqrt{1/2}$, and these values have already been taken into account in equations (1)–(3). The unit vertical wavenumber indicates that the cells extend from top to bottom of the unstable fluid layer, and the constant a shows that their horizontal scale is proportional to h.

The development of solar ponds during the 1970s increased the interest in double diffusive convection, particularly in the presence of non-linear vertical concentration and temperature profiles [3, 4]. Likewise, in recent years it has been recognized that, besides its relevance to oceanographical and technological applications, double diffusive convection plays an important role in geological systems like magma chambers, and in crystallization processes in multicomponent liquids [5, 6]. In any realistic double diffusive system the temperature or concentration gradient can cause

NOMENCLATURE

a	horizontal wavenumber
D	determinant
g	acceleration due to gravity [cm s^{-2}]
h	depth of the layer [cm]
i	imaginary unit, $\sqrt{-1}$
k	coefficient of molecular diffusivity [cm^2 s^{-1}]
M	number of terms in truncated Galerkin series
n	vertical wavenumber
p	complex exponent [s^{-1}]
Pr	Prandtl number, v/k_T
Ra_S	solute Rayleigh number, $(g\beta\Delta Sh^3)/(v_r k_T)$
Ra_T	thermal Rayleigh number, $(g\alpha\Delta Th^3)/(v_r k_T)$
S	salt concentration [frac.]
T	temperature [°C]
x	horizontal coordinate (dimensionless and/or [cm])
z	vertical coordinate (dimensionless and/or [cm]).

Greek symbols

α	coefficient of heat expansion (absolute value) [(°C)$^{-1}$]
β	coefficient of solute expansion (absolute value) [frac.$^{-1}$]
γ	dimensionless dependence of solute diffusivity on temperature, $(dk_s/dT)\cdot\Delta T/k_{S,r}$
ΔS	concentration difference across the layer [frac.]
ΔT	temperature difference across the layer [°C]
δ	Kronecker symbol
ζ	coefficient of viscosity variation
η	ratio, Ra_T^{ζ}/Ra_T^0
θ	dimensionless temperature, $(T-T_r)/\Delta T$
λ	horizontal wavelength, $2\pi h/a$ [cm]
v	kinematic viscosity [cm^2 s^{-1}]
ξ	length scale, $((v_r k_T h)/(g\beta\Delta S))^{0.25}$
σ	dimensionless concentration, $(S-S_r)/\Delta S$
τ	diffusivity ratio, $k_{S,r}/k_T$
ψ	dimensionless stream function.

Subscripts

b	basic state
i	imaginary part
r	reference value; real part
S	salt
T	heat.

Superscripts

0	constant properties case
c	critical value
w	switching point from the direct mode to the oscillatory one.

Other symbols

$\langle\cdot,\cdot\rangle$ scalar product, $\int_0^1 f(z)g(z)\,dz$.

considerable spatial variations of the physical properties of the fluid which, in turn, vary the gradient itself. For example, in a normal solar pond temperature gradient, the kinematic viscosity and salt diffusivity are varied by a factor of three from top to bottom [see equations (4) and (5) below]. Under such circumstances, the assumption of constant properties and linear profiles, and the resulting criteria [e.g. equations (1)–(3)] may not be valid any more. The present investigation was motivated by the conjecture that this assumption can be one of the causes for the discrepancies between the theoretically predicted values of the stability parameters and those observed in real systems [4].

The influence of variable viscosity or variable basic state gradient on the stability of a single diffusive layer (Bénard problem) was studied rather extensively [7–10]. However, to the best of our knowledge the double diffusive stability analysis with variable fluid properties has not been reported in the literature, except for the thesis of Berger [11]. He studied the influence of a linearly variable v, or k_S, or both of them on the critical Ra_T using the assumption of constant salinity and temperature gradients. The related case of variable solute stratification (but constant properties) was studied, using asymptotic [3] and numerical [4] methods. The latter three authors reported that, in the oscillatory mode, the critical thermal Rayleigh number is smaller than its value in the constant gradients case. Walton [3] and Zangrando and Bertram [4] have also shown that, in the oscillatory mode, the instability is localized vertically around the point of minimum salinity gradient.

It should be emphasized that, in the latter three analyses, the basic state is quasi-steady: Berger [11] considered variable k_S (and v) with a constant salinity gradient, while Walton [3] and Zangrando and Bertram [4] studied a non-linear salinity profile with constant properties.

The aim of the present work is to analyze the stability of a steady-state double diffusive layer, *simultaneously* exposed to the effects of variable fluid

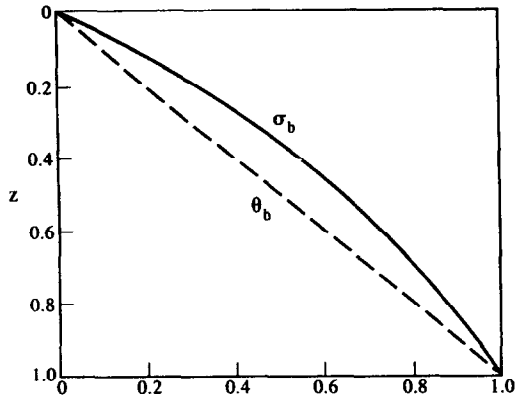

Fig. 1. The basic state non-dimensional profiles of the temperature (θ_b) and concentration (σ_b) as a function of depth (z).

properties and a non-linear basic state salinity distribution. We have taken into account temperature dependent viscosity and salt diffusivity, which leads to the basic state profiles shown in Fig. 1. The stability problem is analyzed numerically using the Galerkin method, widely used for convective stability analyses.

2. FLUID PROPERTIES AND BASIC STATE PROFILES

The ranges of variations of the temperature ($T = 20$–90°C) and salt concentration (S = 0–0.2 in fraction) utilized here are those appropriate for NaCl solar pond conditions. Using literature data [12, 13] it can be shown that, over the above ranges, the variation of ν with temperature is near to 200% while its variation with concentration is about 30%. The corresponding variations of k_S are about 200% and 5%, respectively. The variations of k_T with temperature or concentration are both about 15%. Thus, in the present analysis we have taken into account only the effect of the temperature on ν and k_S, because this effect is the dominant one.

The fluid properties were approximated as:

$$\nu = \exp(-4.098830 - 0.0269082T + 0.991268\times10^{-4}T^2)\ [\mathrm{cm^2\,s^{-1}}] \quad (4)$$

$$k_S = 1.35(1+0.033(T-20))\times10^{-5}\ [\mathrm{cm^2\,s^{-1}}] \quad (5)$$

$$k_T = \text{const.} = 0.0014\ [\mathrm{cm^2\,s^{-1}}]. \quad (6)$$

At the basic state we consider a horizontally infinite stationary fluid layer, stratified by vertical distributions of non-dimensional temperature $\theta_b(z)$ and solute concentration $\sigma_b(z)$, where z is the vertical coordinate axis directed downwards and the subscript 'b' stands for the basic state. The dimensionless steady-state conductive solution with zero velocity is determined by solving the set of coupled equations of heat and salt diffusion, in our case reduced to:

$$\frac{d^2\theta_b}{dz^2} = 0 \quad (7)$$

$$\frac{d}{dz}\left((1+\gamma\theta_b)\frac{d\sigma_b}{dz}\right) = 0 \quad (8)$$

with boundary conditions of fixed temperature and salinity at the upper surface: $z = 0$, $\theta_b(0) = \sigma_b(0) = 0$, and at the lower surface: $z = 1$, $\theta_b(1) = \sigma_b(1) = 1$. The dimensionless variables are defined as $\theta = (T-T_0)/(T_1-T_0)$ and $\sigma = (S-S_0)/(S_1-S_0)$, where the subscripts '0' and '1' correspond to the top and bottom of the layer, respectively. The coordinate z is normalized by the layer depth h and the coefficient γ is

$$\gamma = \frac{\Delta T}{k_{S,r}}\cdot\frac{dk_S}{dT}$$

where $k_{S,r}$ is a reference value of k_S (here at $T = 20^\circ$C).

The system of equations (7) and (8) is solved analytically to obtain:

$$\theta_b = z \quad (9)$$

$$\sigma_b = \frac{\ln(\gamma z+1)}{\ln(\gamma+1)}. \quad (10)$$

The steady basic state profiles of the non-dimensional concentration and temperature are shown in Fig. 1; in the present calculation $\sigma_b = 0.835458\ln(2.31z+1)$.

3. THE SMALL PERTURBATION EQUATIONS

The linearized small perturbation equations are basically similar to those governing the constant properties problem, the difference is the inclusion of terms associated with the temperature dependent viscosity and salt diffusivity in the stream function and concentration equations, respectively. Under the Boussinesq approximation, the density is a linear function of temperature and concentration, and only the effect of its variation on the body force is taken into account. The momentum equation is transformed into the stream function equation and each physical variable is expressed as a sum of its basic state value and a small perturbation. Then the equations are linearized and non-dimensionalized, to yield:

$$\left(\frac{1}{Pr}\frac{\partial}{\partial t} - 2\nu_b'\frac{\partial}{\partial z} - \nu_b\nabla^2\right)\nabla^2\psi + \nu_b''\left(\frac{\partial^2}{\partial x^2} - \frac{\partial^2}{\partial z^2}\right)\psi = Ra_S\frac{\partial\sigma}{\partial x} - Ra_T\frac{\partial\theta}{\partial x} \quad (11)$$

$$\left(\frac{\partial}{\partial t} - \nabla^2\right)\theta = -\frac{\partial\psi}{\partial x} \quad (12)$$

$$\left(\frac{\partial}{\partial t} - \tau(1+\gamma\theta_b)\nabla^2\right)\sigma = \tau\gamma\left(\sigma_b'\frac{\partial\theta}{\partial z} + \sigma_b''\theta + \frac{\partial\sigma}{\partial z}\right) - \sigma_b'\frac{\partial\psi}{\partial x}. \quad (13)$$

In this set of equations ψ, θ and σ are the two-dimensional time-dependent perturbations of the stream function, temperature and concentration, respectively, t is the time and x is the horizontal coordinate. The normalized basic state viscosity $v_b = v/v_r$ is expressed as a function of z, the *prime* symbol denotes the derivative operator d/dz related to functions of single argument and the subscript 'r' denotes a reference constant value. The reference values v_r and $k_{S,r}$ are chosen at $T = 20°C$. To obtain equations (11)–(13), distance was normalized by the layer depth h, time by h^2/k_T, stream function by k_T, and temperature and concentration differences by $\Delta T = T_1 - T_0$ and $\Delta S = S_1 - S_0$. It is also noticed that hereafter τ, Pr, Ra_S and Ra_T are based on v_r and $k_{S,r}$. As usual, positive Ra numbers mean that the layer is heated and salted from below.

The above stability problem is studied under ideal free–free boundary conditions of zero shear stress and zero perturbations at the bottom and top surfaces of the fluid layer:

$$\psi''(x,0) = \psi''(x,1) = 0 \tag{14}$$

$$\psi(x,0) = \psi(x,1) = \theta(x,0) = \theta(x,1) = \sigma(x,0) = \sigma(x,1) = 0. \tag{15}$$

It should be pointed out that shear-free conditions at both top and bottom boundaries are physically unrealistic, and these conditions are utilized here to allow a relatively simple solution of the problem. The following two arguments suggest that using the shear-free boundary conditions instead of the realistic ones would not affect the results significantly (at large Ra_S). First, in the analytical results for the constant-properties and constant-gradient case [see equations (1) and (2)], the constant term on the right-hand side becomes negligible for large Ra_S. This term is associated with the boundary conditions, which implies that at large Ra_S the effect of the boundary conditions on the stability criteria is small. A similar small effect of the boundary conditions can be expected in the present case of variable properties and a non-linear concentration profile. Secondly, when the basic state concentration gradient is variable, the flow pattern at the instability onset is expected to be vertically localized (in particular at large Ra_S, see Section 5.2), and hence less sensitive to the boundary conditions [4].

4. THE NUMERICAL PROCEDURE

To solve our problem we follow the Galerkin method [14]. At the first stage separation of variables is employed in the form:

$$\psi(t,x,z) = f_1(z)\,e^{pt}\sin\pi ax$$

$$\theta(t,x,z) = f_2(z)\,e^{pt}\cos\pi ax$$

$$\sigma(t,x,z) = f_3(z)\,e^{pt}\cos\pi ax$$

where f_1, f_2 and f_3 are some smooth functions, a is a constant and p is in general complex, $p = p_r + ip_i$.

After substituting these expressions into equations (11)–(15), the latter are transformed into a set of ordinary differential equations with the appropriate boundary conditions.

At the second stage, the functions f_i $(i = 1,2,3)$ are expanded into a truncated series on a complete linearly-independent system of functions $\{\sin\pi nz\}$, $(n = 1, M)$, which satisfy the necessary boundary conditions and are orthogonal on the non-dimensional interval $z \in [0,1]$ in the sense of the scalar product

$$\langle f, g\rangle = \int_0^1 f(z)g(z)\,dz.$$

If the expansion series are

$$f_j(z) = \sum_{n=1}^{M} A_{jn}\sin\pi nz \quad (j = 1,2,3)$$

then, using the Galerkin method, the problem is reduced to the following set of homogeneous algebraic equations with $A_{1,n}$ and $A_{3,n}$ as unknowns:

$$\sum_{n=1}^{M} A_{1,n}\left[\pi^3(n^2+a^2)^2\mathbf{I}_0^{n,k} - 2\pi^2 n(n^2+a^2)\mathbf{I}_1^{n,k} + \pi(n^2-a^2)^2\mathbf{I}_2^{n,k} + \tfrac{1}{2}\delta_n^k\left(\frac{\pi p}{Pr}(k^2+a^2) - \frac{a^2\pi\,Ra_T}{\pi^2(k^2+a^2)+p}\right)\right] - a\,Ra_S\frac{A_{3,k}}{2} = 0 \tag{16}$$

$$\sum_{n=1}^{M} A_{1,n}\left[-a\pi\mathbf{S}_{1\#}^{n,k} - \delta_n^k\frac{a\pi\tau\gamma(\pi k\mathbf{S}_1^{k,k} + \mathbf{S}_2^{k,k})}{\pi^2(k^2+a^2)+p}\right] + \sum_{n=1}^{M} A_{3,n}[-\pi^2\tau\gamma((n^2+a^2)\mathbf{T}_0^{n,k} + n\mathbf{T}_1^{n,k}) - \tfrac{1}{2}\delta_n^k(\pi^2\tau(k^2+a^2)+p)] = 0. \tag{17}$$

Here the integer k is running like n from 1 to M, δ_n^k is the Kronecker delta and the following denotations are used:

$$\mathbf{I}_0^{n,k} = \langle v_b\sin\pi nz, \sin\pi kz\rangle$$

$$\mathbf{I}_1^{n,k} = \langle v_b'\cos\pi nz, \sin\pi kz\rangle$$

$$\mathbf{I}_2^{n,k} = \langle v_b''\sin\pi nz, \sin\pi kz\rangle$$

$$\mathbf{T}_0^{n,k} = \langle\theta_b\sin\pi nz, \sin\pi kz\rangle$$

$$\mathbf{T}_1^{n,k} = \langle\theta_b'\cos\pi nz, \sin\pi kz\rangle$$

$$\mathbf{S}_1^{n,k} = \langle\sigma_b'\cos\pi nz, \sin\pi kz\rangle$$

$$\mathbf{S}_{1\#}^{n,k} = \langle\sigma_b'\sin\pi nz, \sin\pi kz\rangle$$

$$\mathbf{S}_2^{n,k} = \langle\sigma_b''\sin\pi nz, \sin\pi kz\rangle.$$

The stability criterion satisfies the requirement $D(Ra_S, Ra_T, a, p) = 0$, where D is the determinant of the homogeneous system (16), (17).

The stability limits for any value of Ra_S are found numerically by searching the minimum of the function $Ra_T(a)$ on the manifold $\{Ra_T | D(Ra_T, a, p) = 0\}$ under

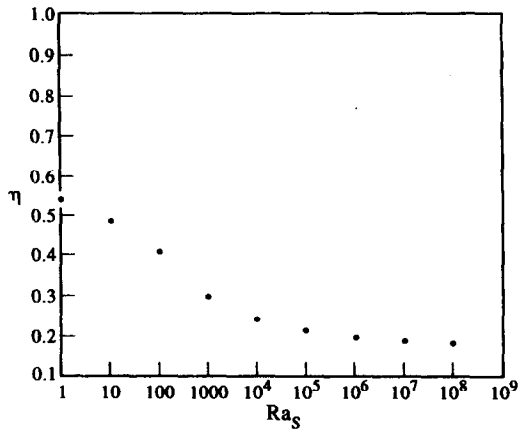

Fig. 2. The ratio $\eta = Ra_T^c/Ra_T^0$ at the onset of direct instability as a function of Ra_S.

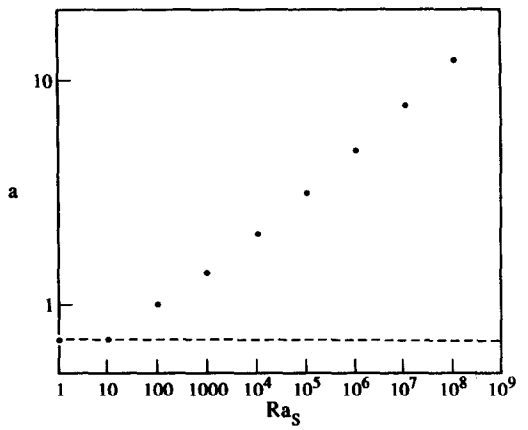

Fig. 3. The wavenumber a at the onset of direct instability as a function of Ra_S. The dashed line indicates the case of constant properties and gradients.

the condition $p = p_r + ip_i = 0$ in the case of direct mode or $p_r = 0$ in the oscillatory mode case. This minimum corresponds to the critical value of $Ra_T = Ra_T^c$ and its associated horizontal wavenumber a. In the second case an additional parameter p_i represents the frequency of marginal oscillations.

All calculations were carried out on the VAX 4000/200 computer at the Center for Technological Education Holon using the software library IMSL.

5. RESULTS AND DISCUSSION

Before analyzing the general double diffusive problem with variable fluid properties and a non-linear salinity profile, the above numerical procedure was validated by analyzing some particular cases, the results of which are already known. Our numerical procedure reproduced very well the stability limits of the particular case of constant properties and gradients, equations (1)–(3), obtained theoretically by several authors (e.g. ref. [2]). These results are used below as references for the variable properties case. Another case utilized to validate our numerical procedure is the Bénard problem with temperature dependent viscosity. Our results are in very good agreement (see the Appendix) with previous ones obtained using a different numerical method.

The results presented below were obtained with the reference values of the variable fluid properties at $T = 20°C$ which yield $Pr = 7.20$, $\tau = 0.0096$ and $\gamma = 2.31$.

5.1. *Direct instability mode*

The resulting stability parameters for the direct mode are presented in Figs. 2 and 3 as a function of Ra_S. The calculated critical thermal Rayleigh number Ra_T^c was divided by Ra_T^0—its value corresponding to the constant properties case [in this case equation (1)]. The resulting ratio $\eta = Ra_T^c/Ra_T^0$ is shown in Fig. 2. The values of η indicate that, for the variable properties case, Ra_T^c is smaller than its value corresponding to constant properties, and the ratio of the two decreases with Ra_S. For example, at $Ra_S = 10$ the value of Ra_T^c is reduced by about 50%, while for $Ra_S > 10^6$, the ratio η decreases to 20% and seems to approach a constant value, independent of Ra_S. This suggests that the asymptotic behavior is $Ra_T^c \propto Ra_S$, as in the case with constant properties and gradients [equation (1) without the second term on the right-hand side]. The same asymptotic behavior was obtained by Zangrando and Bertram [4].

The wavenumber at the onset of direct instability is plotted in Fig. 3. It is shown that the value of the wavenumber a increases with Ra_S in contrast to the constant properties case where $a = \text{const.} = \sqrt{1/2}$. For $Ra_S > 10^3$ the wavenumber is varied as $a \propto Ra_S^{0.18}$ (all exponents displayed hereinafter in *decimal form* have been estimated from our numerical results using the least-squares method). This relation is very close to $a \propto Ra_S^{1/6}$ obtained by Zangrando and Bertram [4] for a cubic concentration profile under constant properties. The proximity of these results suggests that the dominant reason for the variation of a is the nonlinearity of the salinity profile. The variation of a with Ra_S suggests that the dimensional wavelength depends not only on h (as in the case $a = \text{const.}$), but also on the concentration difference ΔS and the fluid properties.

The increase of a, or the decrease of the horizontal wavelength, with Ra_S can be explained physically as follows. In natural convection phenomena, where the flow pattern at the onset of instability is cellular (e.g. Bénard problem), the cells tend to have an aspect ratio of about 1. This is because at the instability onset the potential energy (i.e. the critical ΔT) is minimum and so is the kinetic energy of the fluid. Only cells of aspect ratio close to 1 can persist with this minimum kinetic energy, and therefore this is the preferred geometry. In our case, the concentration gradient is variable and the flow at the onset of convection is expected to occupy only an effective depth of the layer where the concentration gradient is minimum (this is shown in more detail for the oscillatory mode in Section 5.2

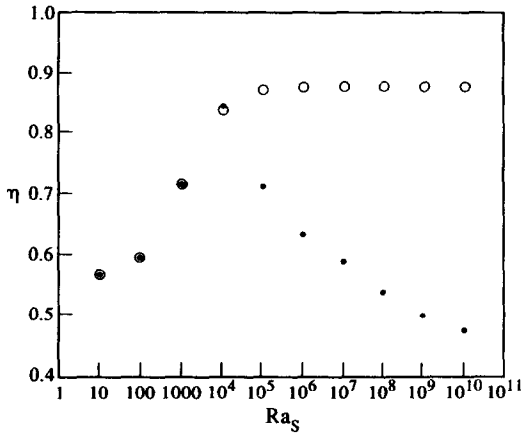

Fig. 4. The ratio $\eta = Ra_T^c/Ra_T^0$ at the onset of oscillatory instability as a function of Ra_S. The two different symbols indicate the different branches for $Ra_S > 4000$.

below). As Ra_S is increased this effective layer depth becomes smaller; the critical cells, however, tend to have an aspect ratio of about 1, and therefore their horizontal wavelength decreases as well.

5.2. *Oscillatory instability mode*

The calculations of the oscillatory instability mode were performed with exactly the same conditions and basic state profiles as those for the direct mode. However, the behavior of this mode, as shown in Figs. 4–6, is somewhat more complex than that in the direct mode case. Essentially, there exists a bifurcation point at $Ra_S \simeq 4000$, from which two separate branches emerge.

Figure 4 shows the calculated values of η for both branches. For the oscillatory mode $\eta = Ra_T^c/Ra_T^0$, where Ra_T^0 is now given due to equation (2). It is observed that, on both branches, the values of Ra_T^c are smaller than the ones for constant properties and gradients. However, one of these branches has lower η values and therefore this branch is the critical one.

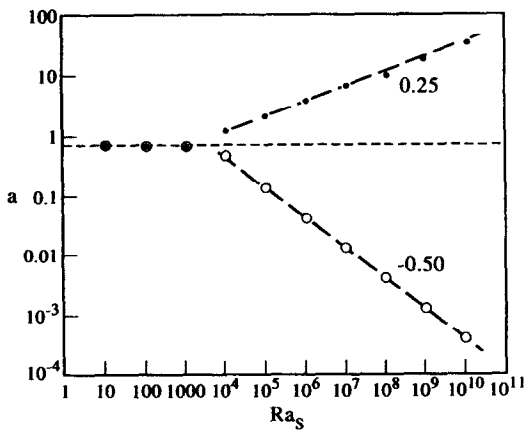

Fig. 5. The wavenumber a at the onset of oscillatory instability as a function of Ra_S. The symbols of the different branches correspond to those in Fig. 4. The horizontal line indicates the case of constant properties and gradients.

The bifurcation is also illustrated by the graph of the wavenumber a at the onset of oscillatory instability, which is shown in Fig. 5. Up to the bifurcation point $a \simeq 0.69$, slightly smaller than its value in the case of constant properties, but afterwards it bifurcates into an increasing and a decreasing branch. On the former the value of a varies like $a \propto Ra_S^{0.25}$, while on the latter $a \propto Ra_S^{-0.50}$. Basically the most unstable branch (the lower one in Fig. 4) corresponds here to higher values of a. However, it seems that at the narrow neighborhood of $Ra_S = 10^4$, the branch with lower a is the critical one, since it has a slightly smaller η. In the analysis of Zangrando and Bertram [4] a region where the branch with lower a is the critical one was also found, but it was much wider, extending from their bifurcation point at $Ra_S \approx 10^4$ up to $Ra_S \approx 10^8$, after which the branch with higher a becomes critical.

On the critical branch $a \propto Ra_S^{0.25}$ and consequently the horizontal wavelength $\lambda = 2\pi h/a$ can be expressed in dimensional variables as

$$\lambda \propto \left(\frac{\nu_T k_T}{g\beta} \cdot \frac{h}{\Delta S}\right)^{0.25} = \xi. \tag{18}$$

This relation indicates that λ does not depend on the layer depth h only, but also depends on the concentration difference (ΔS) and the fluid properties. This result is different from the constant properties and gradients case where $\lambda \propto h$ [2]. Furthermore, since $Ra_S = (h/\zeta)^4$, for $Ra_S > 1$, $\zeta < h$ so that for a fixed layer depth the horizontal wavelength of the unstable motion scales down with increasing Ra_S.

A scale similar to ξ was recently found in the experimental investigation of Kerpel *et al.* [15]. In their experiments a stable constant salinity gradient was heated uniformly from below; a bottom mixed layer is initially formed and on its top secondary layers successively emerge. Kerpel *et al.* [15] have shown that the initial vertical thickness of each secondary layer is proportional to a scale similar to ξ but with k_S replacing k_T. The formation of each secondary layer in that experiment is due to the instability of a horizontal layer stratified by a constant stabilizing salinity gradient and an exponential (and time dependent) destabilizing temperature profile [16]. Although the basic state profiles in such experiments are different from those analyzed here, the agreement between the resulted scales implies that the vertical thickness measured by Kerpel *et al.* [15] is fixed by the horizontal wavelength of unstable oscillations λ (which is proportional to ξ). Zangrando and Bertram [4] have also shown that large horizontal wavenumbers in a solar pond with a variable salinity gradient are associated with vertical localization of the unstable zone. This vertical localization gives rise to the formation of isolated thin horizontal layers in the interior of the pond.

It is noteworthy that a scale similar to ξ was found in three other double diffusive problems. For the hori-

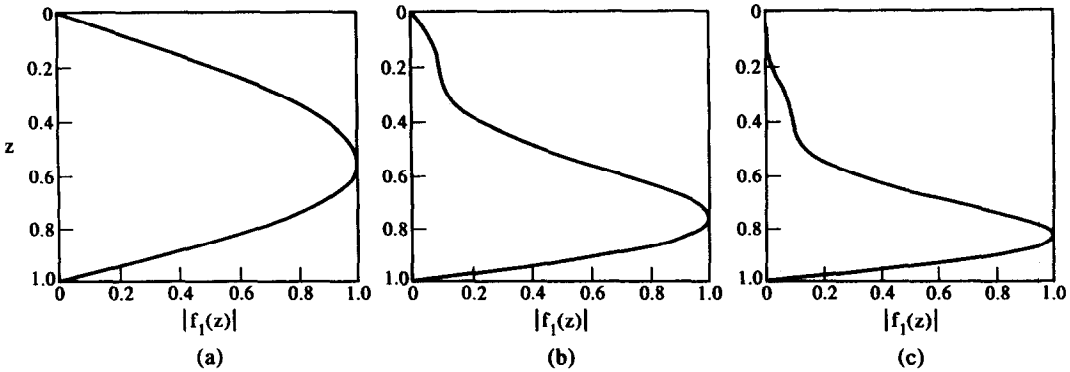

Fig. 6. The normalized amplitude of the stream function perturbation $|f_1(z)|$, as a function of the layer depth z. (a) $Ra_S = 10^3$, $a = 0.69$; (b) $Ra_S = 10^5$, $a = 2.09$; (c) $Ra_S = 10^6$, $a = 3.88$.

zontal layer analyzed here, Stern [17] has shown that the width of salt fingers with maximum growth rate is scaled by ξ, but with the vertical temperature gradient replacing the salinity gradient. Walton [3] has shown that, in an unbounded fluid with constant properties and gradients, the horizontal and vertical wavelengths must be scaled by ξ. The initial layer thickness in the sidewall heating experiments by Tanny and Tsinober [18] was also found to scale with ξ. This diversity implies the universality of this scale in double diffusive phenomena.

The analysis by Zangrando and Bertram [4] was carried out under different conditions from the present ones: the fluid properties were constant while the quasi-steady concentration profile was a cubic with z. Nevertheless Zangrando and Bertram [4] obtained exactly the same relations for the variation of a with Ra_S in the oscillatory mode, namely powers of 1/4 and $-1/2$ for the high and low wavenumber branches, respectively, and a bifurcation point at $Ra_S \simeq 10^4$ (see their Fig. 8a). Thus it is likely that, for these two cases (ours and Zangrando and Bertram's [4]), the characteristic wavelength of oscillatory instability is insensitive to the detailed shape of the concentration profile and to the variability of the fluid properties. One may further conjecture that, in a double diffusive horizontal layer with any kind of a smooth non-linear concentration profile, the wavenumber of the oscillatory mode would be similar to that shown in Fig. 5. This conjecture is not fully supported by Walton's [3] result for a variable salinity gradient, $a \propto Ra_S^{3/14}$; the deviation of the presently calculated power (0.25) from the one calculated by Walton can be explained by the difference between the numerical and asymptotic solution methods.

The ratio η shown in Figs. 2 and 4 indicates that, for both direct and oscillatory mode, the fluid layer with variable properties and a variable salinity gradient would be more unstable than that with constant properties and gradients. This result can be explained by the existence of a region at the bottom of the layer with a salinity gradient which is smaller than the linear one (see the basic state salinity profile in Fig. 1). In this region the layer can become locally unstable at a temperature gradient which is smaller than the one required to destabilize a layer with a linear salinity profile. Hence, the critical value of Ra_T is reduced from that in the case of constant properties and gradients. The reduced Ra_T^c can also be explained by the fact that the viscosity within the layer decreases with temperature. Since the viscosity is a stabilizing factor, a region with smaller viscosity would become locally unstable at a smaller temperature gradient (i.e. a smaller Ra_T^c).

The above physical arguments imply that, when the fluid is heated and salted from below, the unstable motion would be most intense in the lower part of the layer, where both the viscosity and the salinity gradient are smaller. This phenomenon is illustrated in Fig. 6, which shows the vertical distribution of the normalized amplitude of the stream function perturbation (i.e. $|f_1(z)|$, see Section 4) within the layer. This parameter is directly related to the vertical component of the velocity perturbation at the instability onset. The corresponding amplitudes of the temperature and concentration perturbations have basically the same shape as that of the stream function and therefore are not shown here.

It is seen in Fig. 6(a) that, for $Ra_S = 10^3$ (for which $a = 0.69$), the flow essentially occupies the whole layer depth, as in the case with constant properties and gradients. However, Fig. 6(b) shows that, for $Ra_S = 10^5$ (and $a = 2.1$), which is larger than the bifurcation point ($Ra_S \approx 4000$), the perturbation becomes localized vertically, with its maximum amplitude at the lower region of the layer. With a further increase in Ra_S the region with intense motion becomes thinner, as shown in Fig. 6(c) for $Ra_S = 10^6$ and $a = 3.9$.

These observations suggest that, up to the bifurcation point, the variable properties and the nonlinear concentration profile have almost no effect on the structure of the flow, although they considerably reduce the critical Ra_T, as was shown in Fig. 4. However, for $Ra_S > 4000$ (beyond the bifurcation point), the structure of the flow is essentially changed, and the perturbations become localized in the vertical direction. It should be emphasized that the vertical localization observed in Fig. 6 is associated with the

increase of a or the decrease of the critical horizontal wavelength, a phenomenon which was also observed by Zangrando and Bertram [4].

The bifurcation phenomenon observed in Figs. 4 and 5 is of particular interest if one considers realizing this stability problem in the laboratory. For $Ra_S < 4000$ one would expect a single flow pattern at the onset of instability. Beyond the bifurcation point, for $Ra_S > 4000$, two different flow patterns are possible, depending on the actual rate of increase of Ra_T (or the applied ΔT). In this range, for a fixed Ra_S, if Ra_T is increased 'slowly', one would expect instability at the low-η branch (Fig. 4) with a relatively high wavenumber a (Fig. 5). However, if in the experiment ΔT is increased very 'fast', such that the high-η branch is immediately reached, the flow pattern at the instability onset will presumably follow the low-a branch in Fig. 5.

Another important stability parameter is the switch from the direct to the oscillatory mode on the plane Ra_T–Ra_S. For constant properties and for the values of Pr and τ used here, this point is at $Ra_S^w \simeq 0.07$ (here the superscript 'w' denotes the switching point), while for variable properties our calculations indicate $Ra_S^w \simeq 11$. This suggests that, within the range $0.07 < Ra_S < 11$, the direct mode can become critical in a stratification, which—on the basis of the constant properties theory—is favorable to oscillatory instability. Such small values of Ra_S are not of practical interest, but some further calculations revealed that the values of Ra_S, over which such a phenomenon exists, depend strongly on τ. For example, for $\tau \simeq 0.4$ (and the same $Pr = 7.2$), the value of Ra_S^w for constant properties is nearly 180, while in the variable properties case $Ra_S^w > 10^4$, a practically achievable value. The latter result was obtained by increasing $k_{S,r}$ and leaving all other properties unchanged. Although we are presently not aware of a realistic double diffusive system with such a set of properties, it is important to recognize that with variable properties and a non-linear salinity gradient, switching from oscillatory to direct instability can occur at $Ra_S \gg 1$.

The frequency of unstable oscillations is shown in Fig. 7. For the most unstable branch and high a the frequency increases as $Ra_S^{0.53}$, which is similar to the variation found in ref. [4]. It is also noteworthy that on this branch the calculated frequency is very close to the one predicted by the theory for constant fluid properties and gradients, where $p_i \propto Ra_S^{1/2}$ [19]. Thus variable properties and gradients have a very small effect on the frequency of the critical oscillations. For the more stable branch with lower a, our results for $Ra_S > 10^4$ give $p_i = \text{const}$. Zangrando and Bertram [4] also reported a constant frequency on that branch.

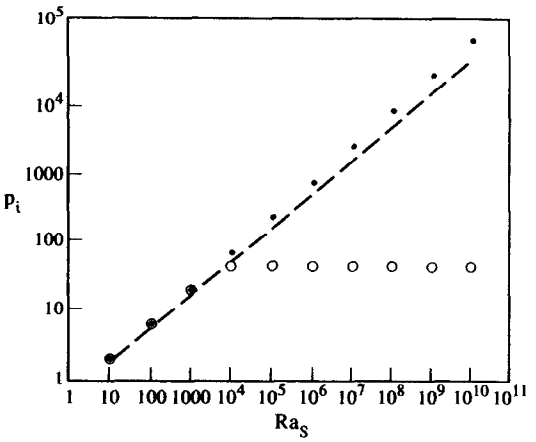

Fig. 7. The frequency p_i at the onset of oscillatory instability as a function of Ra_S. The symbols of the different branches correspond to those in Fig. 4. The dashed line indicates the case of constant properties and gradients.

6. CONCLUSIONS

In this work we have analyzed the linear stability of a horizontal double diffusive layer in which the kinematic viscosity and the coefficient of salt diffusivity are temperature dependent, and consequently the steady basic state salinity distribution is non-linear. The main conclusions of the stability analysis are:

- Variable fluid properties and a non-linear salinity gradient reduce the critical Ra_1 with respect to its constant properties and gradients value, and vary the wavenumber at the onset of instability.
- The stability parameters of the direct mode are characterized by a single critical curve, while for the oscillatory mode bifurcation to two separate branches appears (in the investigated case it occurs at $Ra_S \simeq 4000$).
- For both direct and oscillatory mode, the horizontal non-dimensional wavenumber a at the instability onset increases with Ra_S in contrast to the case of constant properties and gradients where $a = \text{const}$. Hence, the horizontal wavelength depends not only on the layer depth but also on the concentration difference across the layer and on the fluid properties. For the oscillatory mode the increase of a is associated with vertical localization of the flow.
- The variations of the critical wavenumbers and frequencies with Ra_S on the two branches of the oscillatory mode are similar to those found by Zangrando and Bertram [4] for a different basic state salinity profile and for constant properties. This implies that the variable properties affect these stability characteristics mainly through the non-linearity of the basic state profile.

Acknowledgements—We would like to acknowledge Professor A. Tsinober for suggesting the subject to us and for his valuable comments on an earlier draft of the paper. We would also like to acknowledge useful discussions with Dr L. Shtilman. V. A. G. was supported by the Israeli Ministry of Science and Technology under grant no. 3394-1-91 and by the Israeli Ministry of Absorption.

REFERENCES

1. J. S. Turner, *Buoyancy Effects in Fluids*, p. 251. Cambridge University Press, Cambridge (1979).
2. P. G. Baines and A. E. Gill, On the thermohaline convection with linear gradients, *J. Fluid Mech.* **37**, 289–306 (1969).
3. I. C. Walton, Double diffusive convection with large variable gradients, *J. Fluid Mech.* **125**, 123–135 (1982).
4. F. Zangrando and L. F. Bertram, The effect of variable stratification on linear doubly diffusive stability, *J. Fluid Mech.* **151**, 55–79 (1985).
5. H. E. Huppert and R. S. J. Sparks, Double diffusive convection due to crystallization in magmas, *A. Rev. Earth Planet. Sci.* **12**, 11–37 (1984).
6. H. E. Huppert, The intrusion of fluid mechanics into geology, *J. Fluid Mech.* **173**, 557–594 (1986).
7. E. Palm, On the tendency towards hexagonal cells in steady convection, *J. Fluid Mech.* **8**, 183–192 (1960).
8. K. C. Stengel, D. C. Oliver and J. R. Booker, Onset of convection in a variable-viscosity fluid, *J. Fluid Mech.* **120**, 411–431 (1982).
9. D. B. White, The planforms and onset of convection with a temperature-dependent viscosity, *J. Fluid Mech.* **191**, 247–286 (1988).
10. P. C. Matthews, A model for the onset of penetrative convection, *J. Fluid Mech.* **188**, 571–583 (1988).
11. O. Berger, Influence of fluid properties, dependence on temperature, on the stability of solar pond. M.Sc. Thesis, Tel-Aviv University (1983) (in Hebrew).
12. E. E. Washburn, *International Critical Tables of Numerical Data Physics, Chemistry and Technology*, Vol. 5, p. 10. McGraw-Hill, New York (1928).
13. W. Stiles, Indicator method for the determination of coefficients of diffusion, *Proc. R. Soc.* **103**, 260–275 (1923).
14. C. A. J. Fletcher, *Computational Galerkin Methods*. Springer, New York (1984).
15. J. Kerpel, J. Tanny and A. Tsinober, On the secondary layers in a stable solute gradient heated from below, *Fluid Dyn. Res.* **10**, 141–147 (1992).
16. J. S. Turner, The behavior of a stable salinity gradient heated from below, *J. Fluid Mech.* **33**, 183–200 (1968).
17. M. E. Stern, The 'salt fountain' and thermohaline convection, *Tellus* **12**, 172 (1960).
18. J. Tanny and A. Tsinober, The dynamics and structure of double diffusive layers in sidewall heating experiments, *J. Fluid Mech.* **196**, 135–156 (1988).
19. G. Veronis, Effect of a stabilizing gradient of solute on thermal convection, *J. Fluid Mech.* **34**, 315–336 (1968).

APPENDIX: VALIDATION OF THE NUMERICAL PROCEDURE

Our numerical procedure was validated by analyzing the purely thermal Bénard problem with a temperature-dependent viscosity. The comparison was made with the results of Stengel *et al.* [8] for the case of free–free boundary conditions. Following their analysis we have examined a Palm–Jenssen fluid, the viscosity of which depends on temperature as

$$\nu = \nu_r(1 - \zeta \cos \pi(1 - \theta_b))$$

where $\theta_b = \theta_b(z)$ is the dimensionless basic state linear temperature profile, ζ is some constant coefficient and $\nu_r = \nu$ at $\theta_b = 1/2$.

The results of this comparison are shown in Figs. A1 and A2, and one can see the very good agreement between our calculations and those by Stengel *et al.* [8]. The horizontal axis is logarithmically scaled by $\ln(\nu_{max}/\nu_{min})$, the ratio between the maximum and minimum viscosity over the layer, and the vertical axis of Fig. A1 represents η, which was defined before (e.g. Fig. 2). It is noticed that, using a direct method of differential equations integration, Stengel *et al.* [8] could not obtain sufficiently accurate values of the critical wavenumber, while the precision available by our present method is considerably larger. An accuracy like 10^{-6} is fully achievable for reasonable computer time.

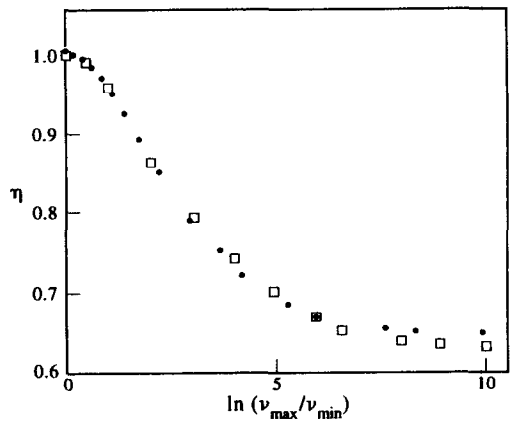

Fig. A1. The ratio η as a function of the viscosity ratio $\ln(\nu_{max}/\nu_{min})$ for Bénard convection with a temperature dependent viscosity. Present calculations ($M = 50$): (•); results of Stengel *et al.* (1982): (□).

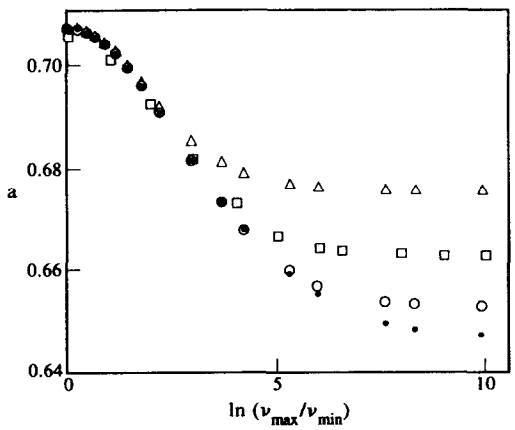

Fig. A2. The wavenumber a at the onset of instability as a function of the viscosity ratio $\ln(\nu_{max}/\nu_{min})$ for Bénard convection with a temperature-dependent viscosity. Present calculations: (△) $M = 3$; (○) $M = 13$; (•) $M = 50$. Results of Stengel *et al.* (1982): (□).

The curves of the wavenumber at instability onset (Fig. A2) show that, for increasing values of the viscosity ratio, convergence is attained using a larger number of terms in the Galerkin expansion. In our problem the ratio $\ln(\nu_{max}/\nu_{min}) \simeq 1$ so that apparently three terms are sufficient for convergence. It turned out however that in the double diffusive problem, more terms are needed for convergence at large Ra_s and therefore most of our calculations were performed with 6–15 terms.